

# Stochastic Security as a Performance Metric for Quantum-enhanced Generative AI

Noah A. Crum,<sup>1,\*</sup> Leanto Sunny,<sup>1,†</sup> Pooya Ronagh,<sup>2,3,4,5,‡</sup>  
Raymond Laflamme,<sup>2,3,4,§</sup> Radhakrishnan Balu,<sup>6,7,¶</sup> and George Siopsis<sup>1,\*\*</sup>

<sup>1</sup>*Department of Physics & Astronomy, The University of Tennessee, Knoxville, TN 37996-1200, USA*

<sup>2</sup>*Institute for Quantum Computing, University of Waterloo, Waterloo, ON, N2L 3G1, Canada*

<sup>3</sup>*Department of Physics & Astronomy, University of Waterloo, Waterloo, ON, N2L 3G1, Canada*

<sup>4</sup>*Perimeter Institute for Theoretical Physics, Waterloo, ON, N2L 2Y5, Canada*

<sup>5</sup>*1QB Information Technologies (1QBit), Vancouver, BC, V6E 4B1, Canada*

<sup>6</sup>*Computer & Information Sciences Directorate, Army Research Laboratory, Adelphi, MD 21005-5069, USA*

<sup>7</sup>*Department of Mathematics, University of Maryland, College Park, MD 20742-4015, USA*

(Dated: February 20, 2025)

Motivated by applications of quantum computers in Gibbs sampling from continuous real-valued functions, we ask whether such algorithms can provide practical advantages for machine learning models trained on classical data and seek measures for quantifying such impacts. In this study, we focus on deep energy-based models (EBM), as they require continuous-domain Gibbs sampling both during training and inference. In lieu of fault-tolerant quantum computers that can execute quantum Gibbs sampling algorithms, we use the Monte Carlo simulation of diffusion processes as a classical alternative. More specifically, we investigate whether long-run persistent chain Monte Carlo simulation of Langevin dynamics improves the quality of the representations achieved by EBMs. We consider a scheme in which the Monte Carlo simulation of a diffusion, whose drift is given by the gradient of the energy function, is used to improve the adversarial robustness and calibration score of an independent classifier network. Our results show that increasing the computational budget of Gibbs sampling in persistent contrastive divergence improves both the calibration and adversarial robustness of the model, suggesting a prospective avenue of quantum advantage for generative AI using future large-scale quantum computers.

**Keywords:** Generative modeling, Energy-based models, Adversarial attacks, Stochastic security, Quantum Gibbs sampling, Diffusion processes, Stochastic gradient Langevin dynamics.

## I. INTRODUCTION

Identifying practical evidence for quantum advantage in quantum machine learning (QML) is a challenging task. Given the astonishing recent pace of advancements in computer vision [1, 2] and language models [3, 4], it remains unclear whether future quantum computers—capable of executing quantum computations fault tolerantly—can outperform classical artificial intelligence (AI) at reasonable cost. In the absence of large-scale quantum computers that can facilitate a direct assessment of any hypothesized revolutionary advances, complexity-theoretic analysis appears to be the only rigorous fallback. However, two main caveats arise when relying on the asymptotic time and space complexity of an algorithm: (a) The complexity of an algorithm often depends not only on the highlighted factors such as the dimensionality of a problem, but also on additional factors (e.g., precision, Lipschitz constants, and smoothness

or convexity measures). (b) An algorithm with seemingly excellent asymptotic complexity can still fail to offer practical advantage, especially on data-driven problems. For example, while the famous simplex algorithm for linear programming has an exponential worst-case complexity, it is in practice preferred over polynomial-time alternatives such as the interior-point method. The situation is even more complex for quantum computing, since any quantum advantage must also be weighed against additional costly resources for protecting the computation from decoherence—such as the energy required for isolation, cooling, and control in cryogenic settings—as well as the overhead of quantum error correction, fault-tolerant protocols, and classical decoding of quantum error-correcting codes.

Recently, [5] analyzed the complexity of solving the Fokker–Planck (or diffusion) equation using quantum ODE (ordinary differential equation) solvers, thereby obtaining a quantum Gibbs sampler for continuous real-valued potentials. For Morse functions (i.e., those with non-singular critical points), and at finite temperatures (the regime of interest in generative AI tasks), this algorithm provides an exponential speedup in the precision, Morseness, and Lipschitz constants of the potential, while increasing the complexity dependence on the dimension of the problem from  $d^3$  to  $d^7$ . At first glance, the slowdown with respect to dimension may seem like a major

---

\* ncrum@vols.utk.edu

† lsunny@vols.utk.edu

‡ pooya.ronagh@uwaterloo.ca

§ laflamme@uwaterloo.ca

¶ rbalu@umd.edu

\*\* siopsis@tennessee.edu

drawback. However, in this paper we show that boosting the precision of a Gibbs sampler can be highly beneficial for enhancing the robustness of the resulting generative AI. We therefore ask whether there are suitable figures of merit for a generative AI model that can serve as quantitative measures for such an assessment. We focus on energy-based models (EBM) in this case study, since a recent resurgence of them has provided state-of-the-art performance in generative AI [6–8]. While it has been hypothesized that EBMs offer improved representations of data in measures such as robustness of the model to adversarial attacks and the calibration of its predictions [7, 9], both training and inference from such models remain bottlenecked by the cost of Gibbs sampling from an energy potential represented by the model network.

In this paper, we propose *adversarial robustness* and *calibration scores* of EBMs trained with a Gibbs sampler (rather than merely the sampling speed) as practical utility measures for assessing the predicted quantum advantage. Adversarial vulnerability is a critical obstacle to the reliable deployment of autonomous agents in sensitive decision making scenarios. [6] and [7] show that EBMs trained via Langevin dynamics exhibit adversarial robustness without explicit adversarial training. It is also important for such agents to be aware of the degree of confidence in their decision, so that they can recognize scenarios in which human expert intervention is required. Although conventional supervised learning models have become more and more accurate in their predictive capabilities, they have also become increasingly less calibrated in their representations [10]. In contrast, [7] shows that EBMs can learn highly calibrated representations of the CIFAR-10 and CIFAR-100 datasets. Other proposed advantages of EBMs include improved mode coverage [6] and better out-of-distribution (OOD) detection [6, 7] compared to the autoregressive and flow-based generative models.

To justify our choice, we numerically study the scaling of these utility measures with respect to the number of iterations of stochastic gradient Langevin dynamics (SGLD) during classical training of an EBM. We provide a primer on EBMs in Section II, and on the quantum Gibbs sampler of [5] in Section III. In Section IV, we use persistent contrastive divergence for classical training of classical EBMs on the CIFAR-10 dataset. Following [9], we diffuse a test image via the trained EBM’s energy potential to purify it from adversarial attacks, before passing it to a classifier network trained completely independently from the EBM. As will be shown, the same diffusion process can also result in more calibrated logits for the classifier. We train a wide residual network (WRN) 28-10 classifier [11], and multiple EBMs using variable numbers of SGLD steps. Our results in Sections V and VI show that purification of samples using EBMs trained with more SGLD steps improves both the adversarial robustness and the calibration of the WRN classifier. We visually observe exponential decays in both the WRN’s adversarial vulnerability and its calibration

error, and quantify these trends using linear regression. Our results provide positive evidence for the utility of efficient Gibbs samplers on continuous potentials, underscoring that the computational bottleneck of EBMs is well worth overcoming using quantum computation.

## II. ENERGY-BASED MODELS

Conventional EBMs, such as Boltzmann machines and Hopfield neural networks [12, 13], and their derivative models [14, 15], are built via undirected graphical models [16, 17]. The neurons represent discrete (binary) random variables and the model’s energy is a function of these discrete random variables (for example, a quadratic binary-valued function representing two-body interactions between the neurons). However, modern EBMs instead use deep neural networks as their underlying graphical models. The deep neural network parametrizes a highly non-convex energy potential defined on a continuous domain (i.e., the continuous signals fed into network’s input layer).

Such EBMs are trained using Monte Carlo integration of Langevin dynamics [6, 18]—a stochastic differential equation (SDE) governing diffusion processes. Alternatively, corrections using the Metropolis–Hastings criteria [19], and second-order variations, such as the Hamiltonian Monte Carlo can be applied [20]. Regardless, these methods for Gibbs sampling require very high numbers of Langevin steps (i.e., the Monte Carlo iterations on the SDE) to approach mixing. Consequently, they are extremely costly and can be numerically unstable in practice. Indeed, many prior works adopt non-convergent shortcuts to training EBMs by collecting short-run Langevin samples [21]. The number of Langevin steps required for training truly convergent EBMs is expected to be at least in the tens of thousands, even for low-resolution image data [18].

An EBM consists of a graphical model that acts as a function approximator for an *energy potential*  $E_\theta : \Omega \rightarrow \mathbb{R}$ . Here  $\theta \in \mathbb{R}^D$  is a vector of  $D$  model parameters,  $\Omega \subseteq \mathbb{R}^d$  is a probability space endowed with a probability measure, and  $d$  represents the dimension of input signals. In this paper we focus on image data without using latent diffusion [2]. Therefore,  $d$  is the number of pixels of the images multiplied by its number of color channels. We also assume pixel intensities are normalized between 0 and 1, so  $\Omega = [0, 1]^d$  throughout. In state-of-the-art diffusion models, high-resolution images are encoded and decoded into much smaller latent spaces, typically with only a few hundred dimensions.

Similar to other ML models, this graphical model is used to determine a *model distribution*. Given a set of i.i.d training samples  $\mathcal{D} = \{x_1, \dots, x_N\} \subset \Omega$  the goal is to learn a vector of model parameters  $\theta^* \in \mathbb{R}^D$  such that the resulting model distribution best approximates an unknown distribution  $p$  from which  $\mathcal{D}$  is assumed to have been sampled. What distinguishes EBMs is that

the model distributions are Gibbs distribution

$$p_\theta(x) = \exp(-\beta E_\theta(x))/Z_{\beta,\theta} \quad (1)$$

of the energy potential. The normalizing constant  $Z_{\beta,\theta} = \int_{x \in \Omega} \exp(-\beta E_\theta(x)) dx$  is the partition function of  $p_\theta$  at thermodynamic constant  $\beta$ . Since the model only determines the energy potential  $E_\theta$  (and not  $p_\theta$  directly) it is called an *unnormalized* probabilistic graphical model. Unlike typical ML models used in discriminative tasks (e.g., classification), EBMs impose no constraints to ensure the tractability of the normalization constant. This makes EBMs more expressive, although it comes at the cost of computational intractability of both training and inference.

The standard method for training probabilistic models from i.i.d. data is maximum likelihood training; i.e., maximizing the expected log-likelihood function over the data distribution,  $\mathbb{E}_{x \sim p}[\log p_\theta(x)]$ . This is equivalent to minimizing the KL distance between  $p_\theta$  and  $p$ , because

$$d_{\text{KL}}(p(x)||p_\theta(x)) = -\mathbb{E}_{x \sim p}[\log p_\theta(x)] + \text{constant}. \quad (2)$$

In fact, we do not require direct access to the likelihood itself but only the gradient of the log-probability of the model. This holds at least for first-order optimization schemes which are the standard techniques for training classical ML models. We have

$$\begin{aligned} \nabla_\theta \log p_\theta(x) &= -\beta \nabla_\theta E_\theta(x) - \nabla_\theta \log Z_{\beta,\theta} \\ &= -\beta \nabla_\theta E_\theta(x) + \beta \mathbb{E}_{x \sim p_\theta}[\nabla_\theta E_\theta(x)]. \end{aligned} \quad (3)$$

In EBMs, the first term above is easily calculated via automatic differentiation, whereas the second term must be approximated through costly Gibbs sampling. Indeed, if we can sample from the model distribution  $p_\theta$ , we obtain unbiased estimates of  $\nabla_\theta E_\theta(x)$ , which we can then leverage to train the EBM via stochastic gradient descent. The overdamped Langevin diffusion

$$dx = -\alpha \nabla_x E_\theta(x) dt + \sigma dW \quad (4)$$

where  $W$  is a standard Wiener process, is known to mix into our desired Gibbs distribution at inverse temperature  $\beta = 2\alpha/\sigma^2$ . Monte Carlo simulation of this SDE is known as stochastic gradient Langevin dynamics (SGLD) and amounts to building discrete time chains

$$\begin{aligned} x_0 &\sim p_0(x), \\ x_{i+1} &= x_i - \alpha \nabla E_\theta(x_i) dt + \varepsilon_i, \quad \varepsilon_i \sim N(0, \sigma), \end{aligned} \quad (5)$$

after a finite number of iterations, where the initial distribution  $p_0$  is typically a uniform distribution.

### III. THE QUANTUM GIBBS SAMPLER

Simulating equilibrium dynamics has long been proposed as a potential application of quantum computers

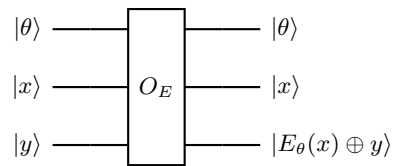


FIG. 1: The oracle for the energy potential. All registers receive float-point representations of real numbers. The first register receives the current model parameters  $\theta \in \mathbb{R}^D$ . The second register receives a data sample  $x \in \Omega \subseteq \mathbb{R}^d$ . And, the third register is used to evaluate the energy potential.

for the past two decades [22–29]. However, these references focus on Gibbs sampling from discrete spin systems, thereby limiting their applicability to traditional EBMs [30–34]. Fortunately, more recent works investigate quantum advantage in Gibbs sampling over continuous domains [5, 35]. [35] considers replacing the classical Monte Carlo simulation of Langevin dynamics with quantum random walks. Consequently, their analysis is limited to convex potentials, which are not relevant to EBMs. However, [5] solves the Fokker–Planck equation (FPE) and prove quantum speedups for highly non-convex potentials. Nevertheless, both of these quantum algorithms require large-scale fault-tolerant quantum computers to train a model with as many parameters as a modest-size modern EBM. Therefore, it is crucial to ask whether a prospective quantum acceleration of continuous-domain Gibbs sampling can serve as a practical motivation for building large fault-tolerant quantum computers.

A quantum Gibbs sampler can replace SGLD as described in Section II both during the training of and inference from an EBM. The neural network of the EBM is a (white-box) composition of affine transformations with nonlinear activation functions. In gate-based quantum computing, one can efficiently construct quantum circuits implementing the arithmetic required for realizing each such function with only a polylogarithmic overhead compared to the gate complexity of the corresponding classical boolean circuit [36]. We can therefore consider a quantum circuit counterpart for the classical deep neural network endowed with a register for input samples  $|x\rangle$  in the computational basis, and another register for receiving the model parameters  $|\theta\rangle$ . Alternatively, the model parameters may be encoded at compile time in a QROM to reduce the qubit count of the circuit [37]. Fig. 1 provides a schematic representation of such a quantum circuit, and will be queried as an *oracle* by the Gibbs sampler. More specifically,  $O(d^2)$  replicas of this circuit are used to construct a controlled unitary operation which is executed repeatedly by the quantum Gibbs sampler. It is important to highlight that unlike most quantum algorithms proposed for classical-data problems, this scheme does not rely on preparing a superposition of classical data in a QRAM, which is extremely costly [38, 39]. Instead, the classical training data is provided iteratively in the computational basis to the  $|x\rangle$  register, similar to

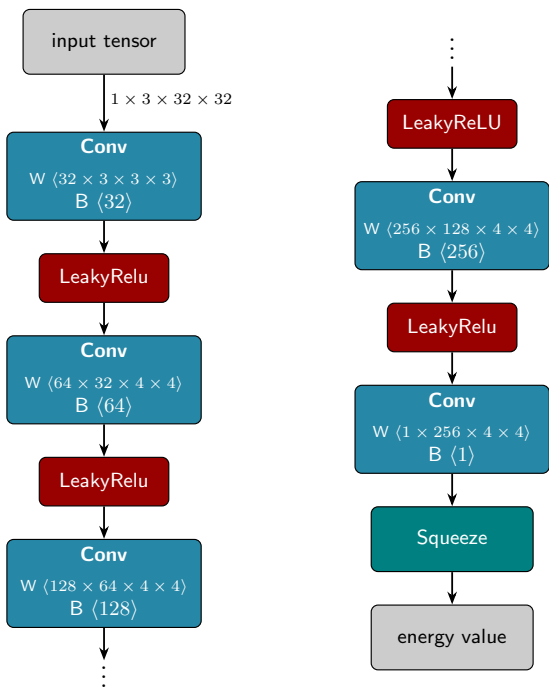


FIG. 2: The EBM architecture of [21]. The neural network parameterizes a real-valued energy function which defines the energy potential used by the quantum Gibbs sampler.

how data is used in classical ML.

For our experiments in Section IV we train the EBM architecture of [21], shown in Fig. 2. Since we do not encode the image in a latent space, the domain of the energy potential has the fairly large dimension of 3072. However, even such a large domain is not beyond the practical reach of QROMs. An educated guess of code distances required with emerging superconducting qubits suggests that code distances below  $\sim 50$  suffice for very large computations [40]. This gives us an estimate of  $\sim 2.5$  million qubits required for a QROM acting on a 3072-wide register of 16-bit float-point numbers. Therefore, we expect these quantum oracles will also be feasible to implement on utility-scale quantum computers. However, we leave a careful and end-to-end resource estimation on our algorithm for future efforts. [5] shows that expanding the FPE in the Fourier basis and solving it via a quantum ODE solver yields high-precision solutions for highly non-convex (but periodic) functions. We now provide a brief and informal summary of the steps of this algorithm.

The Fokker–Planck equation is the PDE (partial differential equation) counterpart to the Langevin SDE of Eq. (4) via the Feynman-Kac formula [41]. While the SDE in Eq. (4) describes the stochastic transitions of a multi-dimensional random variable  $X_t$  attaining values  $x \in \Omega$  as a function of time, the FPE describes the time evolution of the entire probability density function  $\rho_t(x)$  on  $\Omega$  from which  $X_t$  is sampled. The FPE can be written in terms of the second-order differential operator

$\mathcal{L}(-) = \nabla \cdot (e^{-E} \nabla (e^E -))$  as its generator:

$$\frac{d}{dt} \rho_t(x) = \mathcal{L} \rho_t(x). \quad (6)$$

To integrate this equation for time  $T > 0$  with precision  $\varepsilon > 0$ , we discretize the domain  $\Omega$  as a regular lattice  $\mathcal{V}_N$  with  $N = O(d \text{ polylog}(\varepsilon))$  equidistant points along each dimension, and formally replace all differential operators with Fourier derivatives (see Appendix A of [5]) to obtain the linear operator

$$\mathbb{L} : \mathcal{V}_N \rightarrow \mathcal{V}_N \\ \vec{u} \mapsto \tilde{\nabla} \cdot (e^{-E} \tilde{\nabla} (e^E \vec{u})) \quad (7)$$

where tilde signs over the derivatives represent Fourier differentiation, and the arrow over  $u$  indicates that the function is viewed as the long vector of the values it attains on the discrete lattice points.

At an inverse temperature  $\beta > 0$ , a total of  $O(\lambda^{-2} e^{\beta/2} d^7 \text{ polylog}(\varepsilon))$  queries to the energy oracle are required to obtain  $\varepsilon$ -accurate samples from the Gibbs distribution of the energy potential  $E$ , if it is  $\lambda$ -strongly Morse and periodic. These technical conditions are quite tame for machine learning applications since a non-Morse function can be regularized into a Morse one using regularizers and low temperatures  $\beta \rightarrow \infty$  are not desired in generative modeling as they reduce the generalization power of the model. Finally, datasets from non-periodic patterns can be transformed into periodic ones by inverting a trigonometric function of each component, as shown in Fig. 3. Here, each dimension of data is lifted to two branches of the arccos function. Therefore, each sample  $|x\rangle$  in the computational basis corresponds to  $2^d$  inverse images, and an equal superposition  $|\Psi_x\rangle$  of these exponentially many inverse images is efficiently constructed using Hadamard gates. By employing this approach, the resulting energy function learns a consistent periodic potential across all branches of arccos.

#### IV. TRAINING WITH PERSISTENT CHAIN MONTE CARLO

We train several EBMs on the CIFAR-10 dataset [42] using SGLD as described in Section II. The training procedure uses persistent contrastive divergence (PCD)

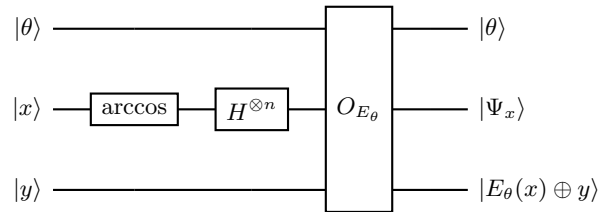


FIG. 3: The oracle of Fig. 1 receiving an augmented sample in superposition as the state  $|\Psi_x\rangle = \sum_{b \in \{0,1\}^d} (-1)^{b_i} \arccos x_i$ .

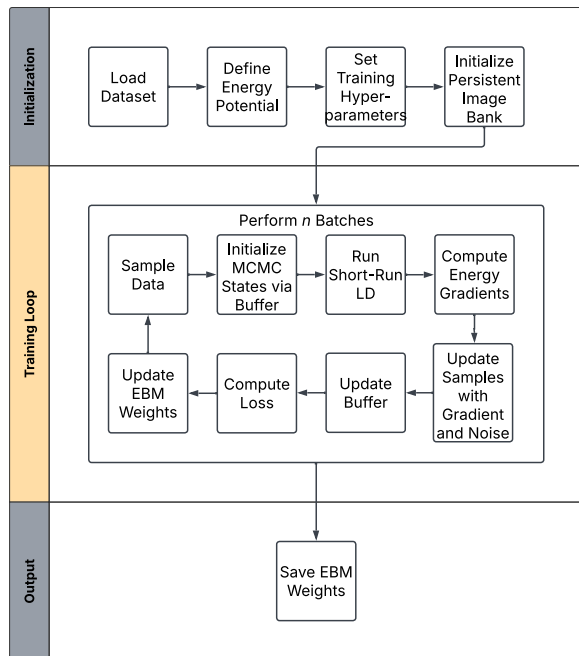


FIG. 4: Training of an EBM using persistent contrastive divergence (PCD) applied to stochastic gradient Langevin dynamics (SGLD). The use of a replay buffer that retains samples from older shorter runs of Langevin dynamics significantly expedites the training process at the cost of creating some instabilities as shown in Eq. (8).

[43], as shown in Fig. 4. Here, a replay buffer retains samples from older, shorter runs of Langevin dynamics. This persistent-chain buffer offers orders-of-magnitude savings in the simulation time of stochastic Langevin dynamics—possibly more than thousands even for small datasets [18]. However, it comes with the cost of increased training instability. Indeed, the distribution,  $\pi$ , representing the persistent chain differs from the true model distribution  $p_\theta$  (the Gibbs distribution). Hence, the update direction followed by  $\theta$  deviates from that of Eq. (2) and must instead be viewed as

$$d_{\text{KL}}(p(x)||p_\theta(x)) - d_{\text{KL}}(\pi||p_\theta(x)). \quad (8)$$

Note that the second divergence is maximized during training. Therefore, the persistent chain distribution diverges from the instantaneous Gibbs state during training, and the faster the model parameters are updated (i.e., with higher learning rate), this deviation increases.

We empirically observed that it is not quite feasible to train such EBMs without PCD. Since we do not reinitialize the persistent chain samples, each PCD sample undergoes all SGLD steps during training, which is proportional to the number of SGLD steps in each epoch of training. Despite the discrepancy in Eq. (8), this value can still be a good indicator of the computational cost of Gibbs sampling for training EBMs.

We train five distinct EBMs with the architecture of Fig. 2, each with a different number of Langevin steps during PCD. Each EBM is trained for 250,000 batches,

beginning with the Adam optimizer [44] and switching to SGD after 125,000 batches with learning rates of 1e-4 and 5e-5 respectively. The change from Adam to SGD has been found to be essential for stable and convergent training of EBMs [21]. Details of the hyperparameters used to train the models are listed in Table I.

## V. ADVERSARIAL ROBUSTNESS

Following [9], we train a prototypical wide residual network (WRN) 28-10 classifier [11]. The classifier is trained for 100 epochs with a scheduled learning-rate decay via SGD on a cross-entropy loss function, with an  $L_2$  regularizer of coefficient 2e-4 for the weights and biases of the model. We denote the classification labels by  $y \in \mathcal{Y} = \{1, \dots, 10\}$ , and for an input image  $x$  we denote the output logits of the classifier by  $f(x)$ . We perform white-box projected gradient descent (PGD) attacks on the classifier [45]. Then we pass the attacked image through Langevin dynamics of the EBMs trained in Section II to purify the image from the attack. We refer the reader to [9, Appendix C] for some theoretical justifications on this method based on the memoryless and chaotic behavior of Markov chain Monte Carlo sampling.

An adversarial attack on a classifier with output logits  $f(x) \in \mathbb{R}^{|\mathcal{Y}|}$  searches for a sample  $x \in [0, 1]^d$  in a neighborhood  $S$  of an attacked image  $x^+$  that maximizes the cross-entropy loss:

$$x_{adv}(x^+, y) = \arg \max_{x \in S} L(f(x), y). \quad (9)$$

The cross-entropy loss  $L(f(x), y)$  is  $-\log(p_y)$  where  $p_y$  is the likelihood of the label  $y$ , obtained by passing  $f(x)$  through the softmax operator.  $S$  is an  $\varepsilon$ -ball around  $x^+$  in the  $L_\infty$ -norm and we have assumed pixel intensities between 0 to 1 for images. The PGD attack scheme is summarized in Fig. 5. The attack starts from a random initial point in  $S$  and maximizes the above objective function via iterative advances along a steepest descent

	WRN classifier	EBMs
Training duration	100 epochs	250,000 batches
Batch size	100	100
Learning rates (LR)	[1e-1, 1e-2, 1e-3]	[1e-4, 5e-5]
LR switch time	Epochs 40 and 60	Batch 125,000
$L_2$ regularizer	2e-4	0
SGLD steps, $n$	-	[50, 75, 100, 150, 200]
SGLD step size, $\alpha$	-	0.01
SGLD noise, $\sigma$	-	0.01

TABLE I: Training hyperparameters. The first column pertains to training of the WRN classifier. The second column reflects the hyperparameters used for training EBMs with varied numbers of SGLD steps.

direction followed by projections back onto  $S$ . That is,

$$x_{i+1} = \Pi_S(x_i + \alpha g(x_i, y)), \quad \text{where} \\ g(x, y) = \arg \max_{\|v\|_\infty \leq 1} v^\top \Delta(x, y). \quad (10)$$

Here  $\Pi_S$  denotes the projection onto  $S$ ,  $\alpha$  is the attack step size, and  $\Delta(x, y)$  is the attack gradient which is  $\nabla_x L(f(x), y)$  in the notation above.

We generate 1,000 adversarial images via PGD attacks on the classifier for various attack strengths  $\varepsilon > 0$ . These images are then diffused through the EBMs using 1,500 Langevin steps for 150 parallel trials. The outputs are provided to the classifier and the logits of all the trials are averaged

$$F(x) \simeq \mathbb{E}_{T(x)}[f(T(x))] \quad (11)$$

to provide a final *post-transformation* label. Here  $T(x)$  represents the random tensor produced after diffusion of  $x$  through Langevin dynamics. This procedure, known as the expectation over transformation (EOT) defense [9], is depicted in Fig. 6.

We perform this procedure using EBMs trained with varying numbers of Langevin steps and demonstrate that longer Langevin sampling improves the adversarial robustness of this defense. As shown in Fig. 7, the standalone classifier is severely vulnerable to PGD attacks, while energy-based purification restores most adversarial images to their original classification labels. In Figs. 8

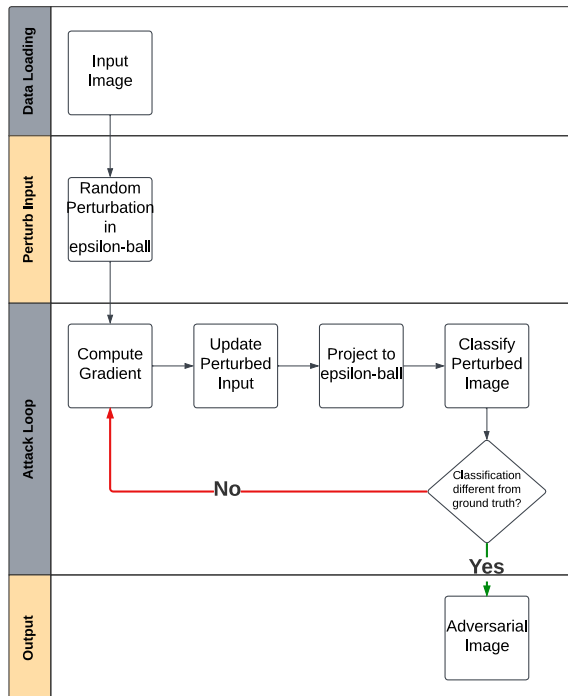


FIG. 5: The projected gradient descent (PGD) attack scheme of [45]. We perform white-box PGD attacks on the classifier. We then pass the attacked image through Langevin dynamics of EBMs to purify it from the attack.

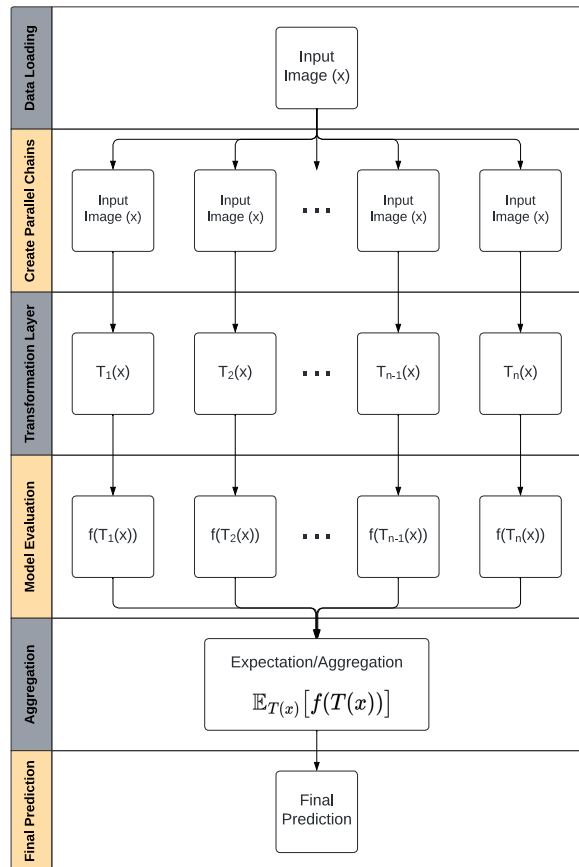


FIG. 6: The schematic of an expectation over transformation (EOT) defense. Attacked images are diffused via an EBM in parallel trials. The outputs are then provided to the classifier and the logits of all the trials are averaged to provide a final post-transformation label.

and 9 we observe that an increase in the duration of Langevin dynamics during EBM training confers greater restorative power, augmenting the model’s ability to distill adversarial signals. We also regress an average exponential decay rate in the classification error across various choices of  $\varepsilon$  and as a function of the number of PCD steps.

The slow rate of this decay suggests that achieving adversarial security may require training EBMs with very large numbers of SGLD steps. For further investigation, we also calculate the relative accuracy error of the defense compared to the original classification error of the model on clean images. Since the goal of purification is to

$255 \times \varepsilon$	0	1	2	3	4	5	6	7	8	9	10	11
$n$	338	300	450	348	380	247	422	655	553	651	503	419

TABLE II: The projected number of SGLD step required for full purification. For each attack strength  $\varepsilon$ , the reported value of  $n$  indicates the predicted number of SGLD steps required during training of the model to restore the classifier back to its original performance with respect to classification of the PGD adversarial images according to regression of a linear trend between the relative classification error and the number of SGLD steps in Fig. 9.

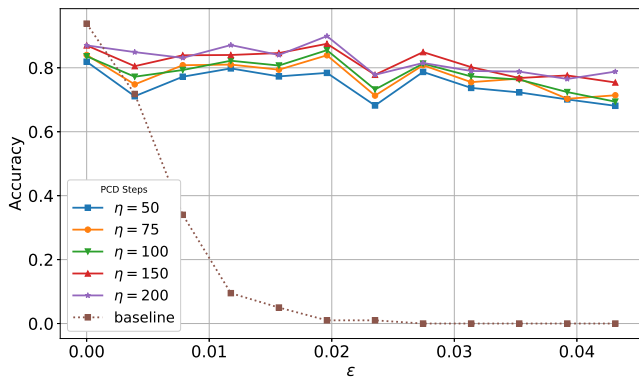


FIG. 7: Classification accuracy versus adversarial attack strength  $\epsilon$ . The ‘baseline’ refers to the classifier unequipped with an EOT defense. The other curves represent the accuracy of the distinct EBMs at classification of 1000 PGD adversarial images after purification and using the post-transformation label as a function of attack strength,  $\epsilon$ .

recover the classifier’s original accuracy on clean images, the relative error is ideally 1 indicating the classifier performs equally well on both clean and adversarial images post-transformation. Table II shows the predicted number of PCD steps, according to the linear fit in Fig. 9, needed during training to allow the EBM to restore the classifier’s performance on post-transformation adversarial images to that of the original classifier for each  $\epsilon$ . We note that a projected runtime for a model utilizing 450 Langevin steps during training in the same fashion as our models is approximately 3.25 days on a single Nvidia Tesla V100S GPU for CIFAR-10 which is not a large dataset.

The EOT defense, itself, gives rise to one of the strongest attacks in the literature known as the EOT attack [46], which exploits access to the classifier logits for a finite number  $m$  of i.i.d. attack samples  $x_1, \dots, x_m \sim$

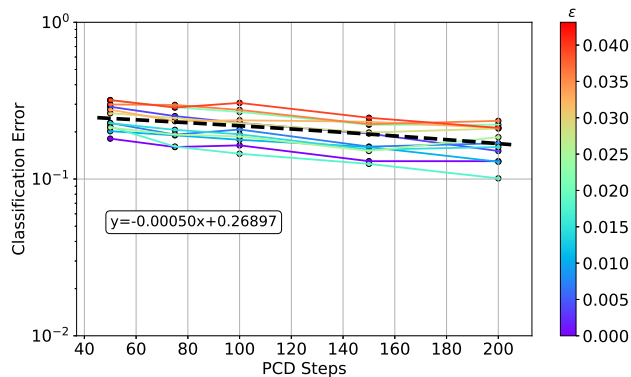


FIG. 8: Post-transformation PGD classification error as a function of the number of SGLD steps of each iteration of training. The color shade of the curves indicate the strength,  $\epsilon$ , of the applied PGD attack.

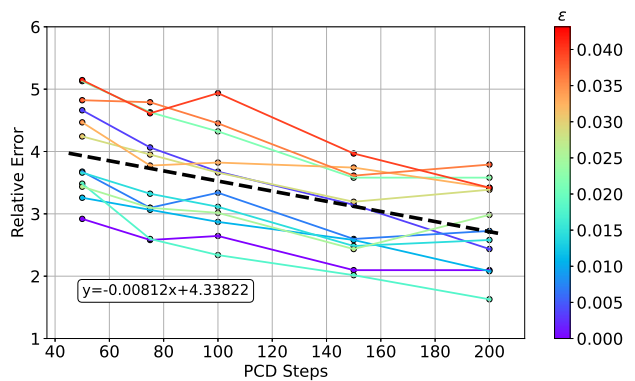


FIG. 9: Classification error relative to the performance of the baseline classifier on clean images. The color shade of the curves indicate the strength,  $\epsilon$ , of the applied PGD attack.

$T(x)$  and the following approximation of  $F(x)$ :

$$\hat{F}_m(x) = \frac{1}{m} \sum_{i=1}^m f(\hat{x}_i). \quad (12)$$

Performing PGD attacks on these logits requires access to derivatives of the diffusion process  $T$  which is overcome using *backward pass differentiable approximation* (BPDA) [46] which in this simplest case approximates the transformation  $T$  via the identity mapping. Therefore PGD will use  $L(f(T(x), y))$  in the forward pass, but use  $\nabla_x L(f(x), y)$  as the attack gradient in the backward pass. Together, the EOT and BPDA give rise to the following attack gradient for PGD:

$$\Delta(x, y) = \frac{1}{m} \sum_{i=1}^m \nabla_{\hat{x}_i} L\left(\frac{1}{m} \sum_{i=1}^m f(\hat{x}_i), y\right). \quad (13)$$

Performing BPDA+EOT attacks is computationally expensive, and therefore the results in Figs. 10 and 11 are restricted to the fixed attack strength of  $\epsilon = 8/255$  (a customary attack strength used in the literature as a benchmark). For these attacks, we report a baseline accuracy

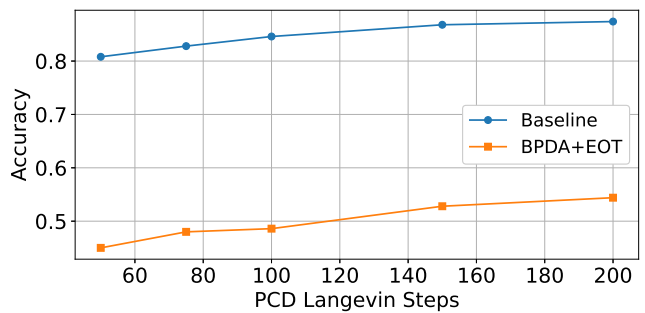


FIG. 10: Prediction accuracy of the EBM and the WRN classifier as a function of SGLD steps used during training after BPDA+EOT attacks. ‘Baseline’ is the pre-attack accuracy, while the other curve shows the post-attack accuracy. The BPDA+EOT attack degrades the performance of the model, however, longer SGLD runs confer greater resistance to the attacks.

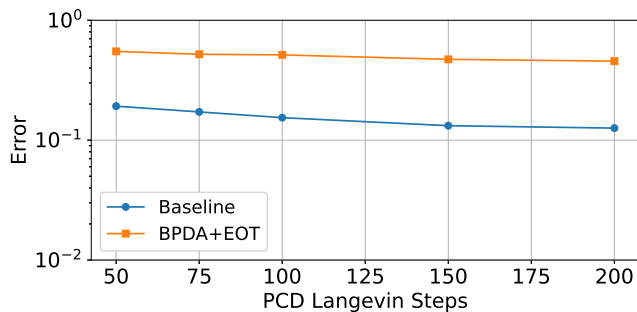


FIG. 11: Classification error after BPDA+EOT attacks in a logarithmic scale as a function of the number of SGLD steps used during training. ‘Baseline’ is the pre-attack accuracy, while the other curve shows the post-attack accuracy.

and prediction error that reflect the pre-attack performance of each EBM–classifier combination. We observe that the baseline model’s classification accuracy improves with longer runs of Langevin dynamics during training. The results of the BPDA+EOT attack are shown on the same plots. Although this attack substantially reduces the classification performance of the joint model, EBMs trained with longer-run Langevin dynamics still demonstrate greater resistance.

## VI. CALIBRATION OF THE MODEL

In addition to improved adversarial robustness, we provide numerical evidence that prolonged PCD during EBM training confer improvements to the calibration of the model as well. Specifically, we study the calibration in the classification of adversarial images, since calibration also pertains to classification capabilities and the standalone EBM is not itself a discriminative model. Calibration indicates that the model’s predictive confidence,  $\max_y p(y|x)$ , is commensurate with its misclassification

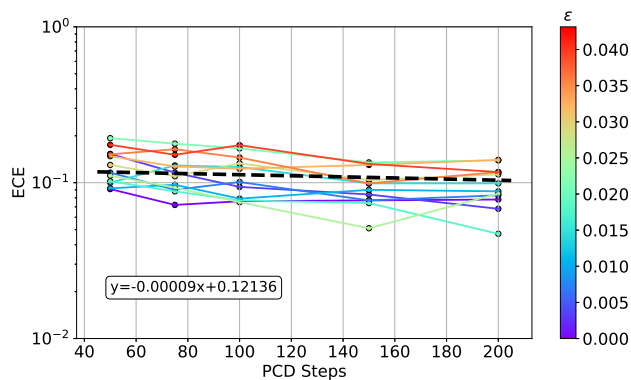


FIG. 12: Expected calibration error (ECE) as a function of the number of SGLD steps executed during the training of EBMs. The ECE calculation pertains to the post-transformation adversarial images. The color shade of the curves shows the strength of the applied PGD attack.

rate. To calculate the expected calibration error (ECE), we find the classification confidence of each sample  $x$  in the dataset, and group them into equally spaced bins,  $\{B_m\}_{m=1}^M$ . For example, with  $M = 20$  bins,  $B_0$  corresponds to all images for which the classifier’s confidence is between 0 and 0.05. The ECE is therefore defined as

$$\text{ECE} = \sum_{m=1}^M \frac{|B_m|}{N} |\text{acc}(B_m) - \text{conf}(B_m)| \quad (14)$$

where  $N$  is in the number of examples in the dataset, and  $\text{acc}(B_m)$  and  $\text{conf}(B_m)$  are respectively the average accuracy and confidence for the samples in bin  $B_m$ .

Fig. 12 shows the ECE of post-purification adversarial images against the number of PCD steps, for each PGD attack strength  $\epsilon$ . The slope of the trend line is indicative of a gradual but steady improvement in the calibration error as the number of PCD steps increases.

## VII. CONCLUSION

A key missing element on the path to fault-tolerant quantum computation is practical utility measures that quantify how transformative the technology will be [47]. Quantum algorithms for solving differential equations can be used to simulate diffusion processes of interest in generative modeling [5–7, 48]. Also, it has been shown that the models trained in this fashion exhibit improved stochastic security [6, 7, 9]. Therefore, in this paper we propose stochastic security as a practical metric for gauging the utility of quantum Gibbs samplers in machine learning tasks.

Because diffusion processes provide the mathematical models of equilibrium and non-equilibrium thermodynamics, they play critical roles in machine learning. The high computational cost of simulating these processes classically—including time, energy, carbon, and water footprint of the computation [49, 50]—has motivated machine learning scientists to critically investigate the practical benefits of models that rely on them. In this paper we focused on deep energy-based models (EBM) as an example from this family [6]. We examined two specific utility measures, namely, the adversarial robustness and calibration of EBMs. The EBMs were trained on classical image data using various amounts of computational budget allocated for performing stochastic gradient Langevin dynamics (SGLD) in order to simulate the diffusion process. After training, diffusion of a test image using the energy potential represented by the trained EBM is used as a transformation that purifies the image from the adversarial attack before presenting it to a wide residual network (WRN) classifier.

Our results demonstrate that purifying samples via EBMs trained with larger numbers of SGLD steps improves the adversarial robustness of the WRN classifier. Interestingly, the same diffusive transformation also yields more calibrated classifications. We visually

observe exponential decays in adversarial vulnerability and calibration error of the WRN, and quantify these trends using linear regression. Overall, our findings offer promising evidence for the practical utility of continuous-domain quantum Gibbs samplers on classical-data problems, all without relying on costly QRAMs.

## ACKNOWLEDGMENTS

This material is based upon work supported by the U.S. Department of Homeland Security through a contract with the Critical Infrastructure Resilience Institute (CIRI) at the University of Illinois. N. A. C., L. S., and G. S. acknowledge support by the U.S. Army Research Office under grant W911NF-19-1-0397 and the U.S. National Science Foundation under grant DGE-2152168. P. R. further acknowledges the support of

NSERC Discovery grant RGPIN-2022-03339, Mike and Ophelia Lazaridis, Innovation, Science and Economic Development Canada (ISED), 1QBit, and the Perimeter Institute for Theoretical Physics. Research at the Perimeter Institute is supported in part by the Government of Canada through ISED, and by the Province of Ontario through the Ministry of Colleges and Universities. This research used resources of the Oak Ridge Leadership Computing Facility, which is a DOE Office of Science User Facility supported under Contract DE-AC05-00OR22725.

The authors thank Simon Verret and Jeff Hnybida for useful discussions. The authors have no conflicts of interest to declare. All authors contributed to the study conception and design. Numerical experiments, analysis of the results, and the generation of figures were performed by N. A. C., and L. S. All authors read and approved the final manuscript.

- 
- [1] A. Ramesh, P. Dhariwal, A. Nichol, C. Chu, and M. Chen, Hierarchical text-conditional image generation with clip latents, arXiv preprint arXiv:2204.06125 (2022).
  - [2] R. Rombach, A. Blattmann, D. Lorenz, P. Esser, and B. Ommer, High-resolution image synthesis with latent diffusion models, in *Proceedings of the IEEE/CVF conference on computer vision and pattern recognition* (2022) pp. 10684–10695.
  - [3] T. Brown, B. Mann, N. Ryder, M. Subbiah, J. D. Kaplan, P. Dhariwal, A. Neelakantan, P. Shyam, G. Sastry, A. Askell, *et al.*, Language models are few-shot learners, *Advances in neural information processing systems* **33**, 1877 (2020).
  - [4] OpenAI, GPT-4 technical report (2023), arXiv:2303.08774 [cs.CL].
  - [5] A. Motamedi and P. Ronagh, Gibbs sampling of continuous potentials on a quantum computer, *Proceedings of Machine Learning Research* **235**, 36322 (2024).
  - [6] Y. Du and I. Mordatch, Implicit generation and generalization in energy-based models, arXiv preprint arXiv:1903.08689 (2019).
  - [7] W. Grathwohl, K.-C. Wang, J.-H. Jacobsen, D. Duvenaud, M. Norouzi, and K. Swersky, Your classifier is secretly an energy based model and you should treat it like one, arXiv preprint arXiv:1912.03263 (2019).
  - [8] Y. Song and D. P. Kingma, How to train your energy-based models, arXiv preprint arXiv:2101.03288 (2021).
  - [9] M. Hill, J. Mitchell, and S.-C. Zhu, Stochastic security: Adversarial defense using long-run dynamics of energy-based models, arXiv preprint arXiv:2005.13525 (2020).
  - [10] C. Guo, G. Pleiss, Y. Sun, and K. Q. Weinberger, On calibration of modern neural networks, in *International Conference on Machine Learning* (PMLR, 2017) pp. 1321–1330.
  - [11] S. Zagoruyko and N. Komodakis, Wide residual networks (2016).
  - [12] D. H. Ackley, G. E. Hinton, and T. J. Sejnowski, A learning algorithm for Boltzmann machines, *Cognitive science* **9**, 147 (1985).
  - [13] J. J. Hopfield, Neural networks and physical systems with emergent collective computational abilities, *Proceedings of the national academy of sciences* **79**, 2554 (1982).
  - [14] G. E. Hinton, S. Osindero, and Y.-W. Teh, A fast learning algorithm for deep belief nets, *Neural computation* **18**, 1527 (2006).
  - [15] G. E. Hinton, Learning multiple layers of representation, *Trends in cognitive sciences* **11**, 428 (2007).
  - [16] D. Koller and N. Friedman, *Probabilistic graphical models: principles and techniques* (MIT press, Cambridge, Massachusetts, 2009).
  - [17] P. Clifford and J. Hammersley, Markov fields on finite graphs and lattices, (1971).
  - [18] E. Nijkamp, M. Hill, T. Han, S.-C. Zhu, and Y. N. Wu, On the anatomy of MCMC-based maximum likelihood learning of energy-based models, in *Proceedings of the AAAI Conference on Artificial Intelligence*, Vol. 34 (2020) pp. 5272–5280.
  - [19] T. Che, R. Zhang, J. Sohl-Dickstein, H. Larochelle, L. Paull, Y. Cao, and Y. Bengio, Your GAN is secretly an energy-based model and you should use discriminator driven latent sampling, *Advances in Neural Information Processing Systems* **33**, 12275 (2020).
  - [20] T. Chen, E. Fox, and C. Guestrin, Stochastic gradient Hamiltonian Monte Carlo, in *International conference on machine learning* (PMLR, 2014) pp. 1683–1691.
  - [21] E. Nijkamp, M. Hill, S.-C. Zhu, and Y. N. Wu, Learning non-convergent non-persistent short-run MCMC toward energy-based model, *Advances in Neural Information Processing Systems* **32** (2019).
  - [22] B. M. Terhal and D. P. DiVincenzo, Problem of equilibration and the computation of correlation functions on a quantum computer, *Physical Review A* **61**, 022301 (2000).
  - [23] D. Poulin and P. Wocjan, Sampling from the thermal quantum Gibbs state and evaluating partition functions with a quantum computer, *Physical review letters* **103**, 220502 (2009).
  - [24] K. Temme, T. J. Osborne, K. G. Vollbrecht, D. Poulin, and F. Verstraete, Quantum Metropolis sampling, Na-

- ture **471**, 87 (2011).
- [25] M. J. Kastoryano and F. G. Brandao, Quantum Gibbs samplers: the commuting case, *Communications in Mathematical Physics* **344**, 915 (2016).
- [26] A. N. Chowdhury and R. D. Somma, Quantum algorithms for Gibbs sampling and hitting-time estimation, *Quantum Info. Comput.* **17**, 41–64 (2017).
- [27] J. Van Apeldoorn, A. Gilyén, S. Gribling, and R. de Wolf, Quantum SDP-solvers: Better upper and lower bounds, *Quantum* **4**, 230 (2020).
- [28] J. Lemieux, B. Heim, D. Poulin, K. Svore, and M. Troyer, Efficient quantum walk circuits for Metropolis-Hastings algorithm, *Quantum* **4**, 287 (2020).
- [29] S. Bravyi, A. Chowdhury, D. Gosset, and P. Wocjan, On the complexity of quantum partition functions, arXiv preprint arXiv:2110.15466 (2021).
- [30] N. Wiebe, A. Kapoor, and K. M. Svore, Quantum deep learning, arXiv preprint arXiv:1412.3489 (2014).
- [31] M. H. Amin, E. Andriyash, J. Rolfe, B. Kulchytsky, and R. Melko, Quantum Boltzmann machine, *Physical Review X* **8**, 021050 (2018).
- [32] D. Crawford, A. Levit, N. Ghadermarzy, J. S. Oberoi, and P. Ronagh, Reinforcement learning using quantum Boltzmann machines, arXiv preprint arXiv:1612.05695 (2016).
- [33] A. Levit, D. Crawford, N. Ghadermarzy, J. S. Oberoi, E. Zahedinejad, and P. Ronagh, Free energy-based reinforcement learning using a quantum processor, arXiv preprint arXiv:1706.00074 (2017).
- [34] B. Sepehry, E. Iranmanesh, M. P. Friedlander, and P. Ronagh, Quantum algorithms for structured prediction, *Quantum Machine Intelligence* **4**, 25 (2022).
- [35] A. M. Childs, T. Li, J.-P. Liu, C. Wang, and R. Zhang, Quantum algorithms for sampling log-concave distributions and estimating normalizing constants, arXiv preprint arXiv:2210.06539 (2022).
- [36] M. A. Nielsen and I. Chuang, *Quantum computation and quantum information* (2002).
- [37] R. Babbush, C. Gidney, D. W. Berry, N. Wiebe, J. McClean, A. Paler, A. Fowler, and H. Neven, Encoding electronic spectra in quantum circuits with linear T complexity, *Physical Review X* **8**, 041015 (2018).
- [38] S. Arunachalam, V. Gheorghiu, T. Jochym-O’Connor, M. Mosca, and P. V. Srinivasan, On the robustness of bucket brigade quantum RAM, *New Journal of Physics* **17**, 123010 (2015).
- [39] O. Di Matteo, V. Gheorghiu, and M. Mosca, Fault-tolerant resource estimation of quantum random-access memories, *IEEE Transactions on Quantum Engineering* **1**, 1 (2020).
- [40] M. Mohseni, A. Scherer, K. G. Johnson, O. Wertheim, M. Otten, N. A. Aadit, K. M. Bresniker, K. Y. Cam-sari, B. Chapman, S. Chatterjee, *et al.*, How to build a quantum supercomputer: Scaling challenges and opportunities, arXiv preprint arXiv:2411.10406 (2024).
- [41] G. A. Pavliotis, *Stochastic processes and applications: diffusion processes, the Fokker-Planck and Langevin equations*, Vol. 60 (Springer, London, UK, 2014).
- [42] A. Krizhevsky, *Learning multiple layers of features from tiny images*, Tech. Rep. (2009).
- [43] T. Tieleman and G. Hinton, Using fast weights to improve persistent contrastive divergence, in *Proceedings of the 26th annual international conference on machine learning* (2009) pp. 1033–1040.
- [44] D. P. Kingma and J. Ba, Adam: A method for stochastic optimization, (2014), cite arxiv:1412.6980 Comment: Published as a conference paper at the 3rd International Conference for Learning Representations, San Diego, 2015.
- [45] A. Madry, A. Makelov, L. Schmidt, D. Tsipras, and A. Vladu, Towards deep learning models resistant to adversarial attacks, arXiv preprint arXiv:1706.06083 (2017).
- [46] A. Athalye, N. Carlini, and D. Wagner, Obfuscated gradients give a false sense of security: Circumventing defenses to adversarial examples, in *International conference on machine learning* (PMLR, 2018) pp. 274–283.
- [47] DARPA, Quantifying utility of quantum computers, Retrieved April 16, 2023, from <https://www.darpa.mil/news-events/2021-04-02> (2021), accessed on April 16, 2023.
- [48] J. Ho, A. Jain, and P. Abbeel, Denoising diffusion probabilistic models, *Advances in Neural Information Processing Systems* **33**, 6840 (2020).
- [49] R. Desislavov, F. Martínez-Plumed, and J. Hernández-Orallo, Compute and energy consumption trends in deep learning inference, arXiv preprint arXiv:2109.05472 (2021).
- [50] P. Li, J. Yang, M. A. Islam, and S. Ren, Making AI less thirsty: Uncovering and addressing the secret water footprint of AI models, arXiv preprint arXiv:2304.03271 (2023).